Annals of Glaciology

Article

Cite this article: Ono J, Komuro Y, Tatebe H (2020). Impact of sea-ice thickness initialized in April on Arctic sea-ice extent predictability with the MIROC climate model. *Annals of Glaciology* **61**(82), 97–105. https://doi.org/10.1017/aog.2020.13

Received: 8 September 2019
Revised: 11 March 2020
Accepted: 12 March 2020
First published online: 21 April 2020

Key words:
Arctic sea ice; ice thickness; initialization; pacific sector; predictability

Author for correspondence:
Jun Ono,
E-mail: junono@aori.u-tokyo.ac.jp

cambridge.org/aog

Impact of sea-ice thickness initialized in April on Arctic sea-ice extent predictability with the MIROC climate model

Jun Ono[1], Yoshiki Komuro[2] and Hiroaki Tatebe[2]

[1]Atmosphere and Ocean Research Institute, University of Tokyo, Chiba, Japan and [2]Japan Agency for Marine-Earth Science and Technology, Kanagawa, Japan

Abstract

The impact of April sea-ice thickness (SIT) initialization on the predictability of September sea-ice extent (SIE) is investigated based on a series of perfect model ensemble experiments using the MIROC5.2 climate model. Ensembles with April SIT initialization can accurately predict the September SIE for greater lead times than in cases without the initialization – up to 2 years ahead. The persistence of SIT correctly initialized in April contributes to the skilful prediction of SIE in the first September. On the other hand, errors in the initialization of SIT in April cause errors in the predicted sea-ice concentration and thickness in the Pacific sector from July to September and consequently influence the predictive skill with respect to SIE in September. The present study suggests that initialization of the April SIT in the Pacific sector significantly improves the accuracy of the September SIE forecasts by decreasing the errors in sea-ice fields from July to September.

Introduction

The Arctic sea-ice cover has decreased in all months since satellite observations began in the late 1970s (Stroeve and Notz, 2018). In particular, sea-ice extent (SIE) in September exhibits a decreasing trend of 12.8% per decade (National Snow and Ice Data Center, 2018, http://nsidc.org/arcticseaicenews/). The decline in Arctic sea ice influences the climate system not only in the Arctic region but also in the midlatitudes (e.g., Mori and others, 2019) and economic activity via the Northern Sea Route (e.g., Khon and others, 2010; Liu and Kronbak, 2010). These factors indicate that there is a need for accurate seasonal-to-interannual sea-ice forecasts (Eicken, 2013).

Initialized predictions using climate models have shown that the summer SIE can be predicted up to 2–7 months ahead (e.g., Sigmond and others, 2013; Wang and others, 2013; Msadek and others, 2014; Bushuk and others, 2017). On the other hand, perfect model ensemble prediction experiments have suggested that the Arctic SIE has a potential predictability of 1–2 years (Blanchard-Wrigglesworth and others, 2011). There is still a gap of a few months to 1 year in the predictable periods between initialized predictions and perfect model experiments. For this reason, further work is needed to improve the forecast accuracy of the real sea ice. The key variables for improving predictive skill are sea-ice thickness (SIT) and subsurface water temperatures (e.g., Day and others, 2014*a*), which are thought to be a memory for sea-ice variability. Hence, the initialization of these physical quantities is very important for seasonal-to-interannual sea-ice forecasts.

Previous studies have pointed out the importance of SIT when predicting the summer sea ice. For example, the SIT in winter to spring is considered to be a key predictor of the SIE in summer (e.g., Kauker and others, 2009; Kimura and others, 2013). The SIT initialization has considerably improved the predictive skill of the Arctic sea ice (e.g., Day and others, 2014*b*; Collow and others, 2015; Dirkson and others, 2017; Blockley and Peterson, 2018; Kimmritz and others, 2018; Zhang and others, 2018). Some studies have also shown that the persistence of SIT could contribute to the skilful prediction of the September SIE (e.g., Bushuk and others, 2017; Ono and others, 2018). However, the sensitivity of the predictions to initializations for different regions for the Arctic sea ice has not yet been thoroughly investigated.

Motivated by the above studies, we investigate the impact of the initialized SIT in April on the predictability of Arctic SIE in September following Day and others (2014*b*) because they did not examine the impact of SIT initialized in spring. To this end, control and perfect model ensemble prediction experiments are first conducted using a climate model, under the Arctic Prediction and Predictability on Seasonal-to-Interannual Time Scales (APPOSITE) project (Day and others, 2016). When performing sea-ice forecasts with coupled global climate models, forecast errors arise from errors in the initial conditions and an incomplete representation of physical processes in the model. In the perfect model experiments, the model can predict itself with ideal initial conditions and no biases (e.g., Collins, 2002). However, it is noted that the predictive skill of a perfect model is not necessarily an upper bound of the predictability, as the climate in the model may be more predictable than in reality or vice versa (Kumar and others, 2014). Second, critical areas for

Table 1. Overview of simulations considered in this study

Experiments	Forcing year	Length	Number of start dates	Start months	Ensemble size	Sea-ice thickness initialization
CTRL	2000	1000 years				
INIT		3 years and 9 months	10	April	8	Yes
CLIM		3 years and 9 months	10	April	8	No
PSINIT		9 months	10	April	8	Only Pacific sector
PSCLIM		9 months	10	April	8	Except for Pacific sector

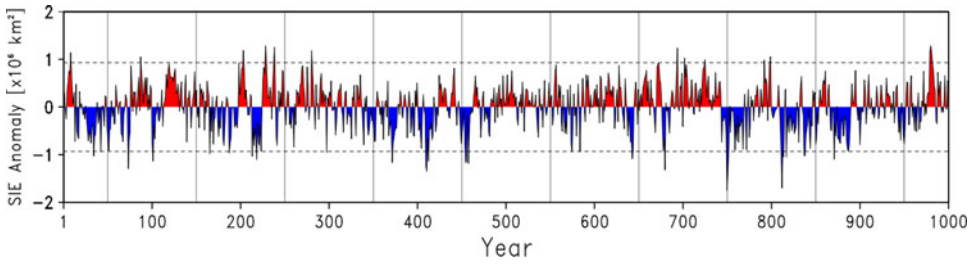

Fig. 1. Time series of the September sea-ice extent (SIE) anomaly relative to the 1000-year climatology of CTRL. Plus and minus two std dev. boundaries are indicated by horizontal dashed lines. Vertical lines denote the ten cases used for perfect model ensemble prediction experiments. Positive anomalies are shown in red and negative in blue.

the improvement of forecast accuracy in the September Arctic SIE are identified based on comparisons of predictability metrics. This will help inform the effective use of the limited ice thickness data for initialization and provide information for target sites focusing on ice thickness observations.

Methods

The climate model used in this study is the Model for Interdisciplinary Research on Climate (MIROC) version 5.2 (Tatebe and others, 2018). The horizontal resolution of the atmospheric component is a T42 spectral truncation (~300 km), and there are 40 vertical levels up to 3 hPa. The warped bipolar horizontal coordinate system of the MIROC5 oceanic component has been replaced by a tripolar coordinate system (Murray, 1996). The horizontal resolution of the oceanic component is a nominal 1° to the south of 63°N and ~60 km over the central Arctic Ocean. There are 62 vertical levels, the lowermost level of which is located at the 6300 m depth. The sea-ice component implements one-layer thermodynamics (Bitz and Lipscomb, 1999), elastic–viscous–plastic rheology (Hunke and Dukowicz, 1997) and a subgrid ice thickness distribution (Bitz and others, 2001) with five categories. The detailed framework and parameters have been described in Komuro and others (2012).

This study is based on perfect model simulations, which is the same approach used in Ono and others (2019). The experiments performed in this study are briefly summarized in Table 1. A control experiment (CTRL) with radiative forcing fixed at present-day levels (year 2000) is conducted following the APPOSITE project framework (Day and others, 2016). The model is newly integrated for 1000 years, arbitrarily labelled 1–1000, with the initial conditions from the CTRL of Ono and others (2019).

A series of perfect model ensemble prediction experiments are carried out to assess the predictability of sea ice. The start date is 1 April of the same year. An ensemble of eight members is generated for the start date. As in Ono and others (2019), only eight ensemble members were used in the perfect model experiments based on the APPOSITE protocol. However, care should be taken when interpreting the results because 10–15 ensemble members are required to effectively capture the internal variability (Jahn and others, 2016). The initial conditions are taken from CTRL, and each member differs only by a perturbation of the sea surface temperature, which is generated by spatially uncorrelated Gaussian noise with a std dev. of 10^{-4} K following the APPOSITE project. Each ensemble is run for 3 years and 9 months from 1 April. The above experiments are referred to as INIT.

Ensemble prediction experiments with the same setup as in INIT but without the initialization of SIT are also conducted following Day and others (2014*b*). To remove the initial memory of the SIT, the grid-averaged SIT is replaced by a climatology for which the monthly mean values during the period of 1–1000 are used, but with the grid-averaged sea-ice concentration (SIC) and snow depth held fixed. The replaced ice thickness for the ith category ($\mathrm{IT}^i_{\mathrm{REPL}}$) is represented as $\mathrm{IT}^i_{\mathrm{REPL}} = \mathrm{IT}^i_{\mathrm{CTRL}} + \frac{\Delta \mathrm{SIT}}{\mathrm{SIC}_{\mathrm{CTRL}}}$, where $\mathrm{IT}^i_{\mathrm{CTRL}}$ is the thickness of the ice for the ith category of CTRL, ΔSIT ($= \mathrm{SIT}_{\mathrm{CLIM}} - \mathrm{SIT}_{\mathrm{CTRL}}$) is the difference in the grid-averaged SIT between the climatology and CTRL, and $\mathrm{SIC}_{\mathrm{CTRL}}$ is the grid-averaged SIC of CTRL. Consequently, the replaced grid-averaged SIT is calculated as $\sum_{i=1}^{5} \mathrm{IC}^i_{\mathrm{CTRL}} \mathrm{IT}^i_{\mathrm{REPL}} (= \mathrm{SIT}_{\mathrm{CLIM}})$, where $\mathrm{IC}^i_{\mathrm{CTRL}}$ is the ice concentration of the ith category of CTRL. However, there is a case where the ice thickness of the ith category is outside of the upper and lower thickness limits (see Table 3 of Komuro and others (2012) for the limits). In that case, the initial values for the ice concentration and thickness, snow depth on ice and temperature in the ice for the ith category are redistributed so that the ith category ice thickness is within the limits. The above experiments are referred to as CLIM. As will be explained in detail later, two additional experiments are also conducted to confirm this paper's hypothesis based on the INIT and CLIM results.

Results

Control experiment

Before showing the results, we briefly review here the basic performance of the model used in this study. As shown in Ono and others (2019), MIROC5.2 largely reproduced the observed features for the mean state, variability and diagnostic predictability of sea ice, indicating that it is a useful model for investigating sea-ice predictability. Note that anomalies for all variables are defined as the deviation from the 1000-year climatology of CTRL. In the present study, we did not consider the climatology

https://doi.org/10.1017/aog.2020.13 Published online by Cambridge University Press

Table 2. September sea-ice extent (SIE) (million km^2) and volume (SIV) (thousand km^3) for 10 model years and their anomalies from the climatology of CTRL (values for the year shown in Figs 4 and 5 are indicated in bold)

Year	51	151	251	351	451	551	651	751	851	951
SIE	6.31	7.36	**6.94**	6.60	6.55	7.27	7.06	**5.81**	6.54	6.73
	−0.68	0.35	**−0.09**	−0.45	−0.53	0.16	−0.07	**−1.35**	−0.65	−0.48
SIV	11.3	17.2	**16.7**	14.8	13.8	15.8	17.6	**12.2**	15.1	14.6
	−4.23	1.44	**0.71**	−1.39	−2.58	−0.79	0.83	**−4.73**	−2.05	−2.73

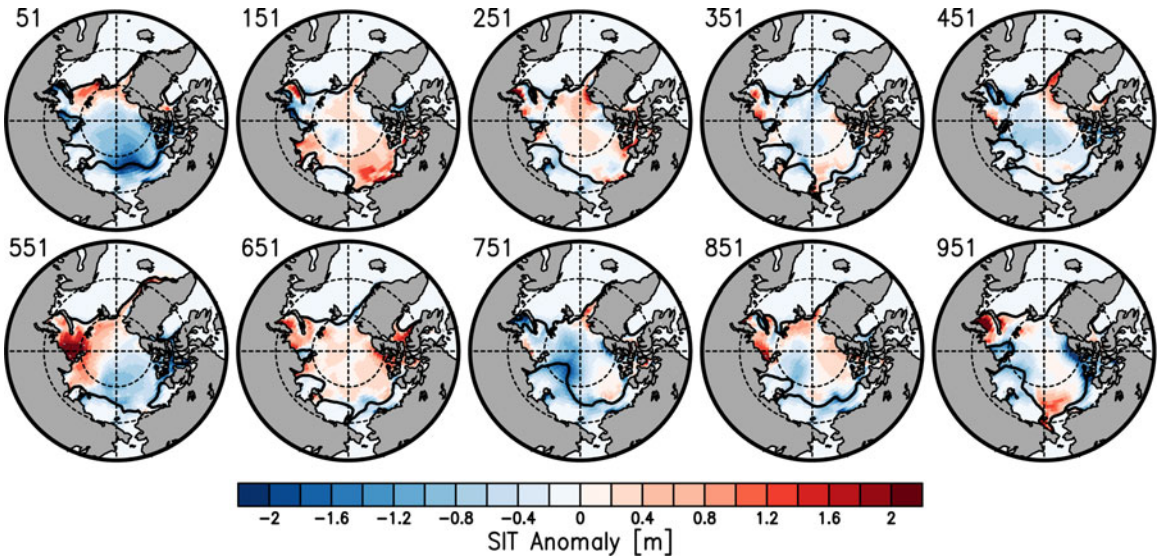

Fig. 2. Sea-ice thickness (SIT) anomalies in September for ten cases in regions from 60 to 90°N. The black lines denote the 15% contours of sea-ice concentration. Dashed lines show latitude 70° and 80° and longitude 0°, 90°, 180° and 270°.

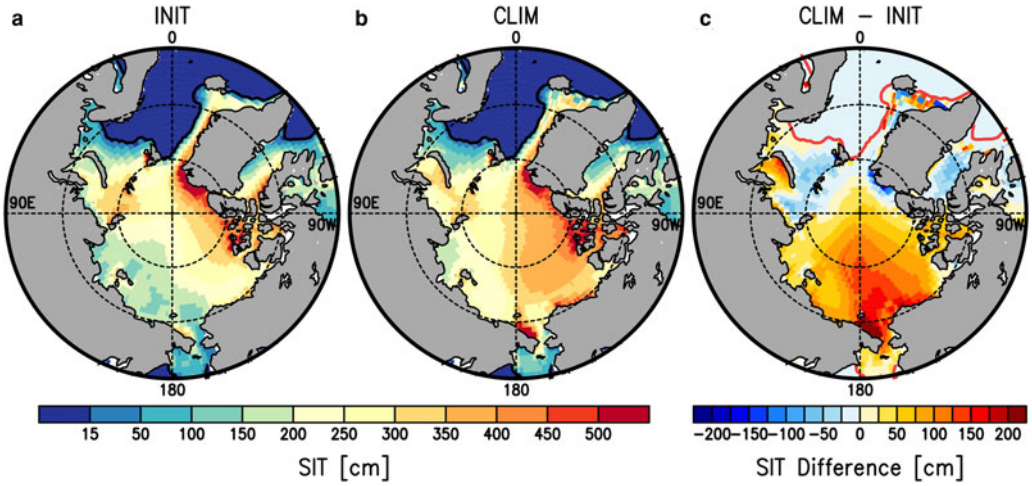

Fig. 3. Sea-ice thickness (SIT) used as an initial value for (a) INIT (1st April 51 model year), (b) CLIM and (c) the difference in sea-ice thickness between INIT and CLIM in regions from 60°N to 90°N (latitude circles of 70°N and 80°N are drawn by dashed circles).

using a shorter window, as suggested by Cruz-García and others (2019), because there is no significant difference in climatology between a 1000-year period and a shorter period (not shown).

Figure 1 shows the time series of the SIE anomaly in September for CTRL. The 1000-year climatology of the CTRL is 7.10 million km^2 and the std dev. is 0.47 million km^2. The interannual variability in SIE is broadly similar to that of the observations, and dozens of extreme anomalies exceeding ± 2 std dev. occur during the 1000 years. A low-frequency variability is also found in the time series, which is characterized by the persistent positive and negative anomalies over the decadal-to-multidecadal timescales. This might be related to longer climate variability, but sea-ice predictability at longer timescales is beyond the scope of this study. For the perfect model ensemble prediction experiments, ten cases will be chosen from CTRL based on the 100-year interval (vertical lines in Fig. 1). There are two positive and eight negative anomalies in SIE from ten cases (Table 2). While the highest SIE is in the model year 151, the anomaly of 0.35 million km^2 is less than one std dev. The lowest SIE is in the model year 751, where the anomaly of −1.35 million km^2, which ranks as the lowest minimum SIE over the 1000 model years, is considerably more than two std dev. below the 1000-year climatology of the CTRL. Among the

https://doi.org/10.1017/aog.2020.13 Published online by Cambridge University Press

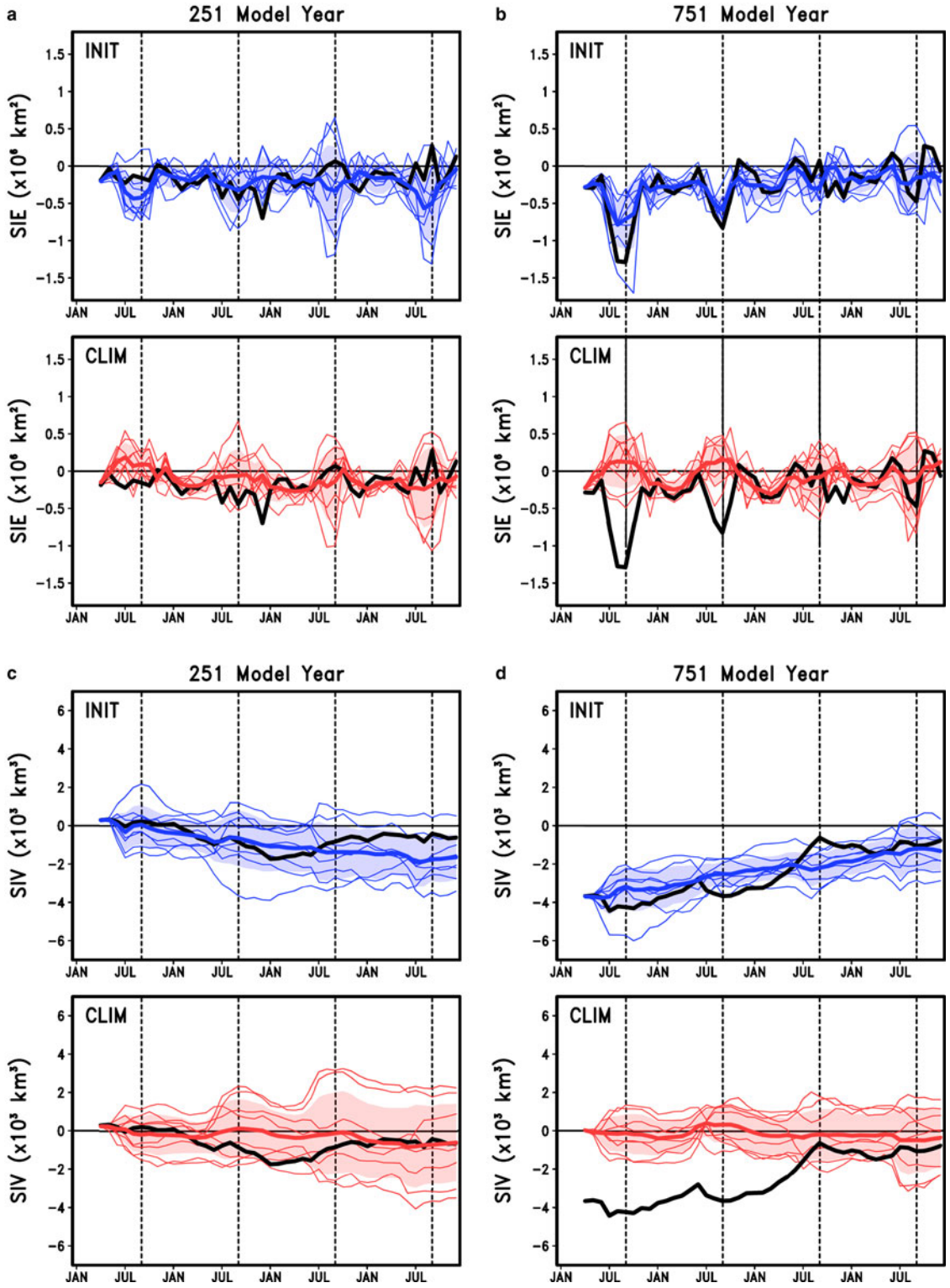

Fig. 4. Time series of sea-ice (a, b) extent (SIE) and (c, d) volume (SIV) anomalies in INIT (blue) and CLIM (red) started from 1 April for model years (a) 251 and (b) 751. Black lines indicate the CTRL results. Blue and red shadings denote the ensemble spread for INIT and CLIM.

ten cases, model years 151 and 751 also have the highest positive and negative anomalies, respectively, in sea-ice volume (SIV).

In most cases for the negative SIE anomalies, the sea ice widely retreats in the Beaufort, Chukchi, East Siberian and Laptev Seas and the thickness anomaly is smaller near the ice edge, especially in model years 51, 751 and 851 (Fig. 2). In contrast, the thickness anomalies in the model year 151 are positive in most areas of the Pacific sector of the Arctic Ocean except for the East Siberian Sea, leading to the positive SIE anomaly. It is likely, at least in MIROC5.2, that the September SIE anomaly is determined by sea-ice variability in the Pacific sector under the influence of the atmospheric circulation anomaly.

Perfect model ensemble prediction experiments

Figure 3 shows the spatial distribution of SIT on 1 April in model year 51 for INIT and CLIM, together with the difference, as an

https://doi.org/10.1017/aog.2020.13 Published online by Cambridge University Press

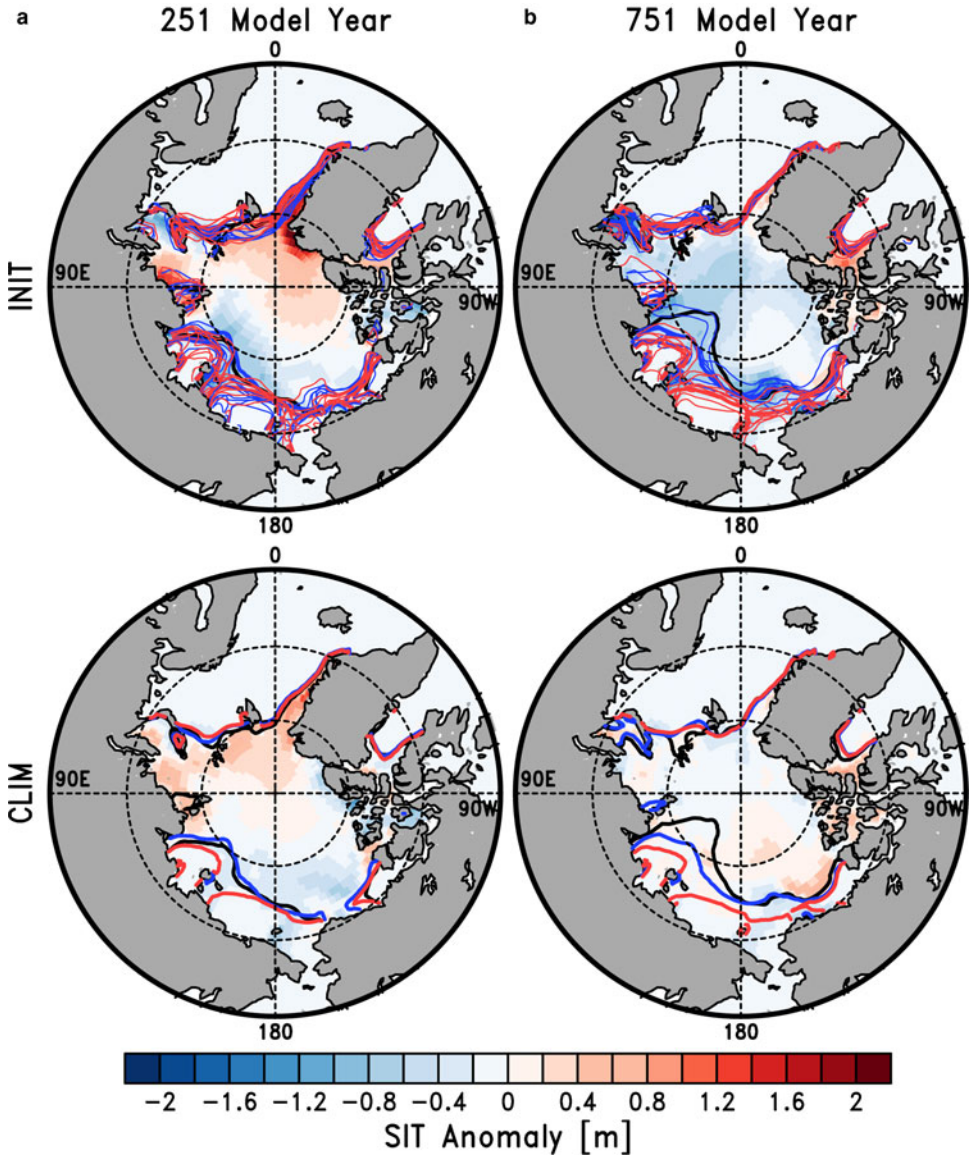

Fig. 5. September sea-ice thickness (SIT) anomaly in INIT and CLIM for model years (a) 251 and (b) 751 in regions from 60°N to 90°N (latitude circles of 70°N and 80° N are drawn by dashed circles). The 15% contours of sea-ice concentration in September are indicated by black, blue and red curves for CTRL, INIT and CLIM, respectively. In INIT for model years 251 and 751, the 15% contours for each ensemble member are also denoted by thin blue (INIT) and red (CLIM) lines.

example of the SIT replacement. The sea ice in CLIM is thicker in the Pacific sector and the western part of the Kara Sea and thinner in the Barents Sea, the northern part of Greenland and the Baffin Bay when compared to INIT.

Before assessing the prediction skill of sea ice, it might be more useful to compare the results in INIT with those in CLIM for a specific model year. Figure 4 shows the time series of the SIE and SIV anomalies for model years 251 (nearly-climatology case) and 751 (highly-extreme case). For the year 251 (Figs 4a and c), the SIE of CTRL remains continuously within the ensemble spread up to the second November (lead month 20) in INIT. In CLIM, it remains within the ensemble spread during the first two lead months (April and May) and freezing seasons (October–March) but not during the first and second melting seasons (April–September). With regard to the SIV, the result of CTRL remains within the ensemble spread over longer lead-times in both prediction experiments because the SIV in the year 251 is close to the climatology. For the year 751 (Figs 4b and d), however, the SIE of CTRL is outside of the ensemble spread in the first September by ~0.2 million km^2 even in INIT. These results are consistent with the previous study by Ono and others (2019), who showed that predictions started in April have no significant skill for a drastic ice reduction in September. In CLIM, the SIE during the melting season is far from CTRL up to the second prediction years. Similar features are also found in the SIV.

Figure 5 shows the spatial distribution of the September SIT anomaly for model years 251 and 751 in INIT and CLIM. For the year 251, the sea-ice edge in CLIM (red line) is inconsistent with those in INIT (blue line) and CTRL (black line) between the East Siberian and the Laptev Seas. These differences lead to the differences in the predictions of the SIE, as shown in Figure 4. For the year 751, even in INIT, the sea-ice retreat lags behind that in CTRL in the northern part of the East Siberian and Laptev Seas (black and blue lines in Fig. 5b). One of the reasons for this is that predictions started on 1 April do not reproduce the Arctic dipole anomaly in sea-level pressure formed in June–August of year 751 (not shown). In contrast, the sea-ice retreat in CLIM is delayed further as a result of the replacement with the thicker climatology, therefore leading to the positive SIE and SIV anomalies.

https://doi.org/10.1017/aog.2020.13 Published online by Cambridge University Press

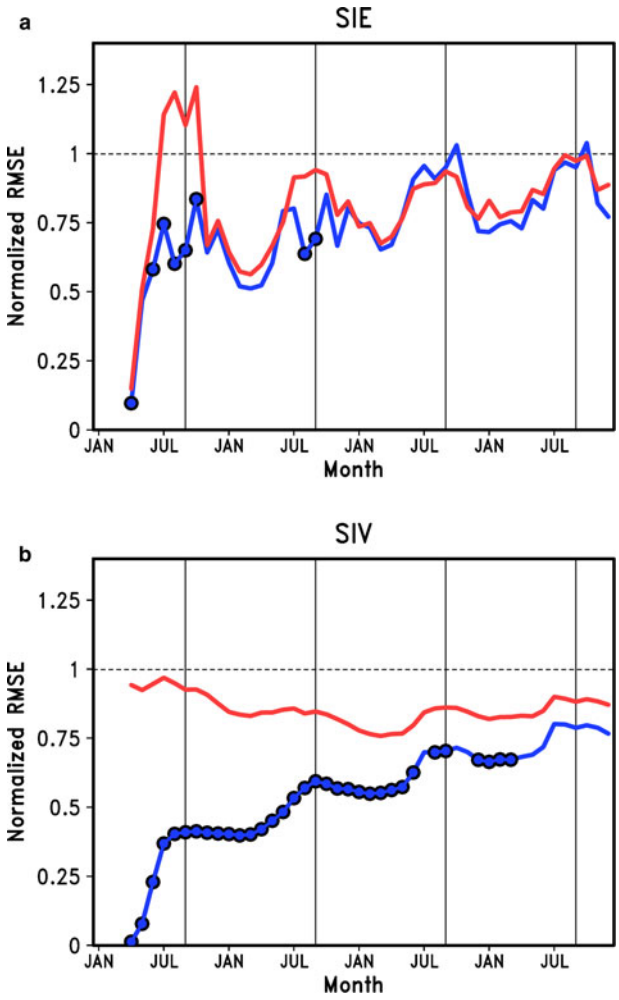

Fig. 6. Time series of the normalized RMSE of sea-ice (a) extent (SIE) and (b) volume (SIV) in INIT (blue) and CLIM (red) initialized on 1 April. Dots indicate where differences between INIT and CLIM are significant at the 5% levels based on a one-sided *F* test.

Next, the prediction skill for SIE and SIV is assessed based on the root-mean-square error (RMSE) presented in Day and others (2014*b*). In perfect model experiments, each ensemble member is assumed to be the truth, and the sufficient sample size can be increased by taking each member in turn as the truth and every other member as a forecast. Therefore, the ensemble RMSE is defined as

$$\mathrm{RMSE}(t) = \sqrt{\frac{\sum_{j=1}^{n_\mathrm{d}} \sum_{i=1}^{n_\mathrm{m}} \sum_{k \neq i} (x_{kj}(t) - x_{ij}(t))^2}{n_\mathrm{d} n_\mathrm{m} (n_\mathrm{m} - 1)}},$$

where x_{ij} (t) is a certain variable (such as SIE) at lead time t for the ith member of the jth ensemble, n_d $(=10)$ is the number of start dates, and n_m $(=8)$ is the number of ensemble members. The state is said to be predictable at lead time t, if RMSE $(t) < \sqrt{2}\sigma$ where σ is the climatological std dev. of CTRL (Collins, 2002). As in Day and others (2014*b*), the RMSE of INIT is calculated in such a way that x_{kj} is considered to be the truth and each x_{ij} the forecast. Similarly, the RMSE of CLIM is calculated by replacing x_{ij} in the above equation with y_{ij}, which is the equivalent member from CLIM. The difference between these two RMSE values gives the gain in skill between the climatological and perfect initialization of the SIT field. The significance of the difference is calculated based on an *F* test with n_d $(n_\mathrm{m} - 1) = 70$ degrees of freedom.

Figure 6 shows the time series of the normalized RMSE of SIE and SIV (normalized by $\sqrt{2}\sigma$) in INIT and CLIM, which were initialized on 1 April. The normalized RMSE in CLIM (Fig. 6a) exceeds 1.0 from June (lead month 3) to October (lead month 7), and thus SIE in September is not predictable. In contrast, the INIT predictions indicate that SIE is continuously predictable up to the third September (lead month 30). A significant difference between them is found in lead months 3–7 (Fig. 6a), which is somewhat better than the predictions started on 1 January in Day and others (2014*b*). This difference is likely impacted by April being a shorter lead time than January. In this study, there are also significant differences in the second August and September. This is likely because of the summer-to-summer re-emergence mechanism associated with the persistence of ice thickness (Day and others, 2014*b*). Similarly, there are significant differences in SIV over longer lead times, compared to those in SIE, as in Day and others (2014*a*). As shown in Cruz-García and others (2019), since the autocorrelation structure of SIV in MIROC (also see Fig. 3c in Ono and others (2019)) is larger than in other models, there is the potential for unrealistically high SIV predictability. Therefore, the predictability of SIV in INIT and CLIM might be influenced by the autocorrelation structure of SIV in MIROC.

Focusing on the first forecast year (lead months 1–9 or April–December), we investigate the area underlying the prediction skill of the September SIE. Figure 7 shows the spatial distribution of the difference in the RMSE of SIT and concentration between INIT and CLIM. For the SIT RMSE, the difference for the first lead month (April) is significant in most regions of the Arctic Ocean. In the fourth to sixth lead months (July–September), the difference in SIT RMSE decreases except for the Pacific sector (Fig. 7a). For the SIC RMSE, there are no significant differences in most of the Arctic Ocean in the first 3 months (April–June). During lead months 4–6 (July to September), the differences become significant in the Beaufort, Chukchi, East Siberian and Laptev Seas (Fig. 7b). Initial errors in the April SIT cause errors in the July to September SIC in the Pacific sector and influence the prediction skill of the September SIE. Therefore, the initialization of ice thickness in the Pacific sector is thought to be crucial. These results are supported by Ono and others (2018), who found a significant relationship between the September SIE and the sea-ice fields in the Pacific sector during the melting season. Additionally, the impacts of initializing predictions with different SIT in April on other variables are shown in Figure S1. Significant differences in RMSE are found in most of the Pacific sector, where the differences in SIC and SIT RMSE are significant (Fig. 7).

To confirm whether the thickness of April sea-ice fields in the Pacific sector of the Arctic Ocean determines the September SIE variability, two additional ensemble prediction experiments started on 1 April with the SIT initialization only in (PSINIT) and except for (PSCLIM) the Pacific sector (the area enclosed by thick lines shown in Fig. 8c) are conducted until the first December (lead months 9). The normalized SIE RMSE of PSINIT (green line) is generally consistent with that of INIT (blue line), except for lead months 1 and 3 (April and June), indicating that the September SIE is predictable (Fig. 8a). The normalized SIE RMSE of PSCLIM (black line) is larger than that of INIT (blue line), as in CLIM (red line). In contrast, the normalized SIV RMSE is significantly higher in both PSINIT (green line) and PSCLIM (black line) than in INIT (blue line) up to lead months 9 (Fig. 8b). From these results, the RMSE in the sea-ice fields of PSINIT is expected to be small compared to CLIM. In fact, in PSINIT (Figs 8c and d), differences in the RMSE of SIC and SIT in September (lead months 6) decrease substantially in the Pacific sector

https://doi.org/10.1017/aog.2020.13 Published online by Cambridge University Press

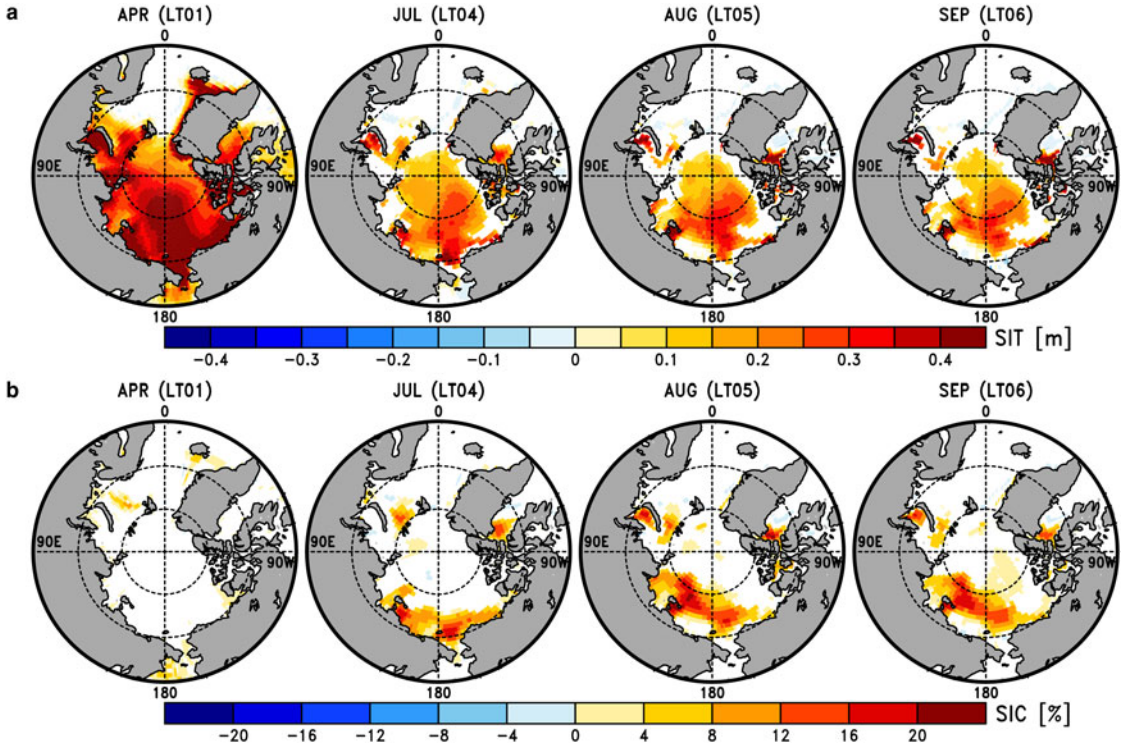

Fig. 7. Spatial distribution of the difference in the RMSE of sea-ice (a) thickness (SIT) and (b) concentration (SIC) in April (lead month 1), July (lead month 4), August (lead month 5) and September (lead month 6) in regions from 60°N to 90°N (latitude circles of 70°N and 80°N are drawn by dashed circles). All coloured grid points are significant at the 5% level based on a one-sided *F* test.

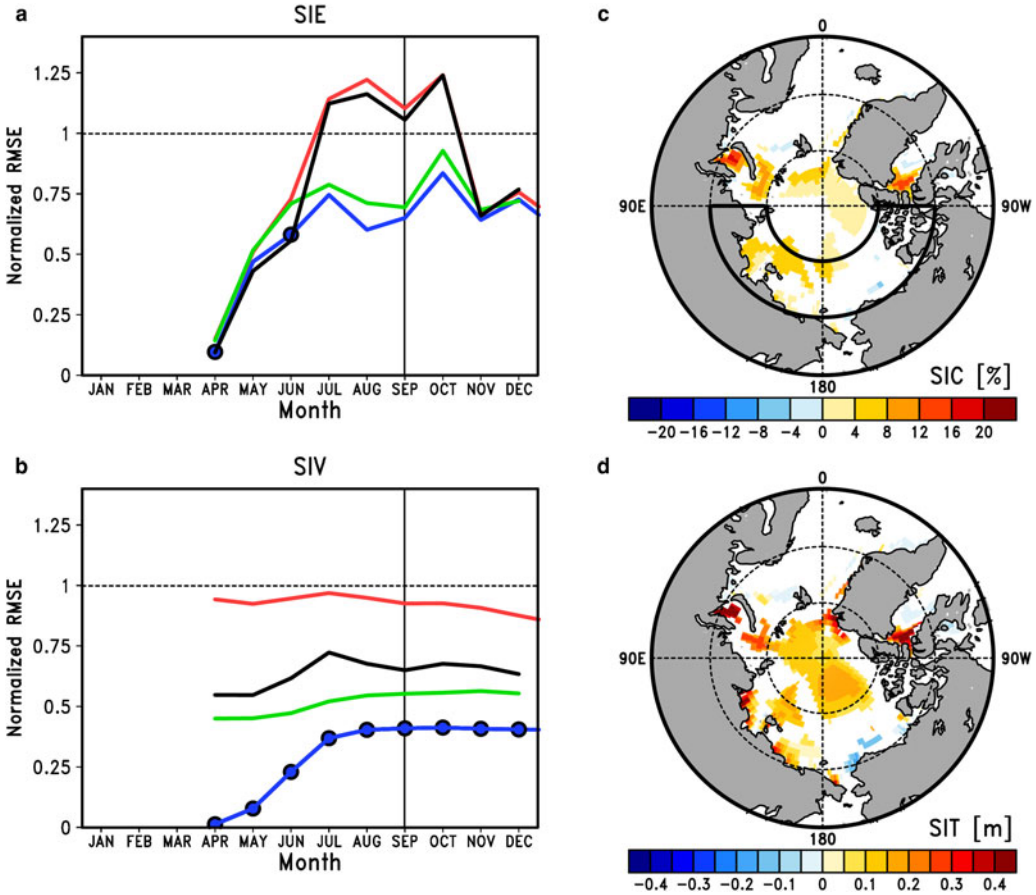

Fig. 8. Time series of the normalized RMSE of sea-ice (a) extent and (b) volume in INIT (blue), CLIM (red), PSINIT (green) and PSCLIM (black) initialized on 1 April. Blue dots indicate where differences between INIT and PSINIT are significant at the 5% levels based on a one-sided *F* test. Spatial distribution of the difference in the RMSE of sea-ice (c) concentration (SIC) and (d) thickness (SIT) in September (lead month 6) between INIT and PSINIT in regions from 60°N to 90°N (Latitude circles of 70°N and 80°N are drawn by dashed circles). All coloured grid points are significant at the 5% level based on a one-sided *F* test. The area enclosed by thick lines is the region of the Pacific sector considered in this study.

https://doi.org/10.1017/aog.2020.13 Published online by Cambridge University Press

when compared to CLIM (Figs 7a and b). As pointed out in previous studies (e.g., Bushuk and others, 2017; Ono and others, 2018), the persistence of sea ice is the source of predictability for the September SIE. These results therefore suggest that initialization of the April SIT only in the Pacific sector improves the forecast accuracy of the September SIE.

Concluding Remarks

The present study investigated the impacts of initialization of SIT in April on Arctic sea-ice predictability and further identified the critical areas for the skilful forecasts of the September SIE. To this end, following partly Day and others (2014*b*), a series of perfect model ensemble prediction experiments were conducted using climate model MIROC5.2. Ensembles with initialization of the April SIT can predict the September SIE for greater lead times than those without initialization – up to 2 years ahead. SIT correctly initialized in April leads to the skilful prediction of SIE in the first September due to the persistence of SIT (Fig. S2). We also speculate that a summer-to-summer re-emergence mechanism contributes to the prediction skill in the second September. On the other hand, the incorrect initialization of SIT in April results in errors in the SIC and thickness in the Pacific sector from July to September and consequently influences the prediction skill of the SIE in September. Our results suggest that the initialization of the SIT in the Pacific sector significantly improves the forecast accuracy of SIE by decreasing the errors in sea-ice fields from July to September.

Incorporating accurate sea-ice observations for forecast initialization is an important step in making skilful seasonal sea-ice forecasts. Production centres routinely assimilate available satellite-derived and in situ atmosphere and ocean observations and SIC. However, SIT data are not currently available from May to September each year (e.g., Tilling and others, 2016). For other months, these data do not go back far enough to initialize a sufficient number of hindcasts to provide robust estimates of predictive skill. The present study showed the effectiveness of SIT initialization in April when the observed data are available (e.g., Ricker and others, 2014), as shown in previous studies (Day and others, 2014*b*; Yang and others, 2016; Chen and others, 2017; Mu and others, 2017; Blockley and Peterson, 2018; Kimmritz and others, 2018). Furthermore, our results suggest that the critical region for sea-ice initialization is the Pacific sector. If the initialization of ice thickness only in a specific region of the Arctic Ocean is found to improve the regional predictability of sea ice, from the viewpoint of cost performance, it will be useful for planning observational campaigns as well as developing forecast systems.

Meanwhile, large-scale Arctic sea-ice circulations are dominated primarily by the Beaufort Gyre (BG) and the Transpolar Drift Stream (TDS) (e.g., Kwok and others, 2013). Considering the sea-ice advection, the initialization of thickness is expected to be sufficient in upstream regions. However, predictions initialized in the Pacific sector (PSINIT in this study) include a substantial contribution from the BG and TDS. It is therefore unclear how initial SIT in the upstream of the BG and TDS contributes to errors in the Pacific sector via advection as well as melting processes. This point needs to be addressed in future work.

Supplementary material. The supplementary material for this article can be found at https://doi.org/10.1017/aog.2020.13.

Acknowledgements. This work was a part of the Arctic Challenge for Sustainability (ArCS) Project (Program Grant Number JPMXD1300000000). Jun Ono was supported by the Japan Society for the Promotion of Science (JSPS) Grant-in-Aid for Young Scientists (B) 17K12830. Numerical experiments were conducted on the Earth Simulator at the Japan Agency for Marine-Earth Science and Technology (JAMSTEC). We thank the two anonymous reviewers and scientific editor Dr David Babb for their useful comments and suggestions.

References

Bitz CM, Holland MM, Weaver AJ and Eby M (2001) Simulating the ice-thickness distribution in a coupled climate model. *Journal of Geophysical Research* **106**, 2441–2463.

Bitz CM and Lipscomb WH (1999) An energy-conserving thermodynamic model of sea ice. *Journal of Geophysical Research* **104**, 15669–15677.

Blanchard-Wrigglesworth E, Bitz CM and Holland MM (2011) Influence of initial conditions and climate forcing on predicting Arctic sea ice. *Geophysical Research Letters* **38**, L18503. doi: 10.1029/2011GL048807

Blockley EW and Peterson KA (2018) Improving Met Office seasonal predictions of Arctic sea ice using assimilation of CryoSat-2 thickness. *The Cryosphere* **12**, 3419–3438. doi: 10.5194/tc-12-3419-2018

Bushuk M and 6 others (2017) Skillful regional prediction of Arctic sea ice on seasonal timescales. *Geophysical Research Letters* **44**, 4953–4964. https://doi.org/10.1002/2017GL073155

Chen Z, Liu J, Song M, Yang Q and Xu S (2017) Impacts of assimilating satellite sea ice concentration and thickness on Arctic sea ice prediction in the NCEP Climate Forecast System. *Journal of Climate* **30**, 8429–8446. https://doi.org/10.1175/JCLI-D-17-0093.1

Collins M (2002) Climate predictability on interannual to decadal time scales: the initial value problem. *Climate Dynamics* **19**, 671–692. doi: 10.1007/s00382-002-0254-8

Collow TW, Wang W, Kumar A and Zhang J (2015) Improving Arctic sea ice prediction using PIOMAS initial sea ice thickness in a coupled ocean–atmosphere model. *Monthly Weather Review* **143**, 4618–4630. https://doi.org/10.1175/MWR-D-15-0097.1

Cruz-García R, Guemas V, Chevallier M and Massonnet F (2019) An assessment of regional sea ice predictability in the Arctic ocean. *Climate Dynamics* **53**, 427–440. https://doi.org/10.1007/s00382-018-4592-6

Day JJ and others (2016) The Arctic predictability and prediction on seasonal-to-interannual timescales (APPOSITE) data set version 1. *Geoscientific Model Development* **9**, 2255–2270. doi: 10.5194/gmd-9-2255-2016

Day JJ, Hawkins E and Tietsche S (2014*b*) Will Arctic sea ice thickness initialization improve seasonal-to-interannual forecast skill? *Geophysical Research Letters* **41**, 7566–7575. doi: 10.1002/2014GL061694

Day JJ, Tietsche S and Hawkins E (2014*a*) Pan-Arctic and regional sea ice predictability: initialization month dependence. *Journal of Climate* **27**, 4371–4390. doi: 10.1175/JCLI-D-13-00614.1

Dirkson A, Merryfield WJ and Monahan A (2017) Impacts of sea ice thickness initialization on seasonal Arctic sea ice predictions. *Journal of Climate* **30**, 1001–1017. doi: 10.1175/JCLI-D-16-0437.1

Eicken H (2013) Arctic Sea ice needs better forecasts. *Nature* **497**, 431–433.

Hunke EC and Dukowicz JK (1997) An elastic-viscous-plastic model for sea ice dynamics. *Journal of Physical Oceanography* **27**, 1849–1867.

Jahn A, Kay JE, Holland MM and Hall DM (2016) How predictable is the timing of a summer ice-free Arctic? *Geophysical Research Letters* **43**, 9113–9120. https://doi.org/10.1002/2016GL070067

Kauker F and 5 others (2009) Adjoint analysis of the 2007 all time Arctic sea-ice minimum. *Geophysical Research Letters* **36**, L03707. doi: 10.1029/2008GL036323

Khon VC, Mokhov II, Latif M, Semenov VA and Park W (2010) Perspectives of Northern Sea Route and Northwest Passage in the twenty-first century. *Climatic Change* **100**, 757–768. https://doi.org/10.1007/s10584-009-9683-2

Kimmritz M and 5 others (2018) Optimising assimilation of sea ice concentration in an Earth system model with a multicategory sea ice model. *Tellus A* **70**, 1435945. doi: 10.1080/16000870.2018.1435945

Kimura N, Nishimura A, Tanaka Y and Yamaguchi H (2013) Influence of winter sea-ice motion on summer ice cover in the Arctic. *Polar Research* **32**(1), 20193. doi: 10.3402/polar.v32i0.20193

Komuro Y and Others (2012) Sea-ice in twentieth-century simulations by new MIROC coupled models: a comparison between models with high resolution and with ice thickness distribution. *Journal of the Meteorological Society of Japan* **90A**, 213–232. doi: 10.2151/jmsj.2012-A11

Kumar A, Peng P and Chen M (2014) Is there a relationship between potential and actual skill? *Monthly Weather Review* **142**, 2220–2227. https://doi.org/10.1175/MWR-D-13-00287.1

Kwok R, Spreen G and Pang S (2013) Arctic Sea ice circulation and drift speed: decadal trends and ocean currents. *Journal of Geophysical Research* **118**, 2408–2425. doi: 10.1002/jgrc.20191

Liu M and Kronbak J (2010) The potential economic variability of using the Northern Sea Route (NSR) as an alternative route between Asia and Europe. *Journal of Transport Geography* **18**, 434–444. https://doi.org/10.1016/j.jtrangeo.2009.08.004

Mori M, Kosaka Y, Watanabe M, Nakamura H and Kimoto M (2019) A reconciled estimate of the influence of Arctic sea-ice loss on recent Eurasian cooling. *Nature Climate Change* **9**, 123–129. https://doi.org/10.1038/s41558-018-0379-3

Msadek R, Vecchi GA, Winton M and Gudgel G (2014) Importance of initial conditions in seasonal predictions of Arctic sea ice extent. *Geophysical Research Letters* **41**, 5208–5215. doi: 10.1002/2014GL060799

Mu L and 6 others (2017) Improving sea ice thickness estimates by assimilating CryoSat-2 and SMOS sea ice thickness data simultaneously. *Quarterly Journal of the Royal Meteorological Society* **144**, 529–538. https://doi.org/10.1002/qj.3225

Murray RJ (1996) Explicit generation of orthogonal grids for ocean models. *Journal of Computational Physics* **126**, 251–273.

National Snow and Ice Data Center: Arctic Sea Ice News & Analysis, available at: http://nsidc.org/arcticseaicenews/, last access: 1 September 2019.

Ono J, Tatebe H and Komuro Y (2019) Mechanisms for and predictability of a drastic reduction in the Arctic sea ice: APPOSITE data with climate model MIROC. *Journal of Climate* **32**, 1361–1380. doi: 10.1175/JCLI-D-18-0195.1

Ono J, Tatebe H, Komuro Y, Nodzu MI and Ishii M (2018) Mechanisms influencing seasonal to inter-annual prediction skill of sea ice extent in the Arctic Ocean in MIROC. *The Cryosphere* **12**, 675–683. doi: 10.5194/tc-12-675-2018

Ricker R, Hendricks S, Helm V, Skourup H and Davidson M (2014) Sensitivity of CryoSat-2 Arctic sea-ice freeboard and thickness on radar-waveform interpretation. *The Cryosphere* **8**, 1607–1622. doi: https://doi.org/10.5194/tc-8-1607-2014

Sigmond M, Fyfe JC, Flato GM, Kharin VV and Merryfield WJ (2013) Seasonal forecast skill of Arctic sea ice area in a dynamical forecast system. *Geophysical Research Letters* **40**, 529–534. doi: 10.1002/grl.50129

Stroeve J and Notz D (2018) Changing state of Arctic sea ice across all seasons. *Environmental Research Letters* **13**, 103001.

Tatebe H, Tanaka Y, Komuro Y and Hasumi H (2018) Impact of deep ocean mixing on the climate mean state in the Southern Ocean. *Scientific Reports* **8**, 14479. doi: https://doi.org/10.1038/s41598-018-32768-6

Tilling RL, Ridout A and Shepherd A (2016) Near-real-time Arctic sea ice thickness and volume from CryoSat-2. *Cryosphere* **10**, 2003–2012. https://doi.org/10.5194/tc-10-2003-2016

Wang W, Chen M and Kumar A (2013) Seasonal prediction of Arctic sea ice extent from a coupled dynamical forecast system. *Monthly Weather Review* **141**, 1375–1394. doi: 10.1175/MWR-D-12-00057.1

Yang Q and 5 others (2016) Taking into account atmospheric uncertainty improves sequential assimilation of SMOS sea ice thickness data in an ice-ocean model. *Journal of Atmospheric and Oceanic Technology* **33**, 397–407. https://doi.org/10.1175/JTECH-D-15-0176.1

Zhang YF and 7 others (2018) Insights on sea ice data assimilation from perfect model observing system simulation experiments. *Journal of Climate* **31**, 5911–5926. https://doi.org/10.1175/JCLI-D-17-0904.1

https://doi.org/10.1017/aog.2020.13 Published online by Cambridge University Press